Applied Physics
Express

LETTER • OPEN ACCESS

Nonvolatile magneto-thermal switching driven by vortex trapping in commercial In-Sn solder

To cite this article: Poonam Rani *et al* 2025 *Appl. Phys. Express* **18** 033001

OPEN ACCESS

Applied Physics Express 18, 033001 (2025) LETTER

https://doi.org/10.35848/1882-0786/adb6ee

Nonvolatile magneto-thermal switching driven by vortex trapping in commercial In-Sn solder

Poonam Rani[1*], Takumi Murakami[1], Yuto Watanabe[1], Hossein Sepehri-Amin[2], Hiroto Arima[1,3], Aichi Yamashita[1], and Yoshikazu Mizuguchi[1*]

[1]Department of Physics, Tokyo Metropolitan University, 1-1, Minami-osawa, Hachioji, 192-0397, Japan
[2]National Institute for Materials Science, 1-2-1, Sengen, Tsukuba, 305-0047, Japan
[3]National Institute of Advanced Industrial Science and Technology, 1-1-1 Umezono, Tsukuba 305-8563, Japan

*E-mail: jangrapoonam622@gmail.com; mizugu@tmu.ac.jp

Received November 25, 2024; revised February 2, 2025; accepted February 16, 2025; published online March 6, 2025

Magneto-thermal switching (MTS) is a key technology for efficient thermal management. Recently, large MTS with nonvolatility has been observed in Sn-Pb solders [H. Arima et al. Commun. Mater. 5, 34 (2024)] where phase separation, the different superconducting transition temperatures (T_c) of Sn and Pb, and magnetic-flux trapping are the causes of the nonvolatile MTS. To further understand the mechanism and to obtain the strategy for enhancing switching ratio, exploration of new phase-separated superconductors with nonvolatile MTS is needed. Here, we show that the In52-Sn48 commercial solder is a phase-separated superconducting composite with two T_c and traps vortices after field cooling. A clear signature of nonvolatile MTS was observed at $T = 2.5$ K. From specific heat analyses, we conclude that the vortices are mainly trapped in the lower-T_c phase (γ-phase) after field cooling, which is evidence that vortex trapping also works on achieving nonvolatile MTS in phase-separated superconducting composites.

Supplementary material for this article is available online

Superconductivity is a quantum phenomenon that emerges at low temperatures. At temperatures (T) lower than the superconducting transition temperature (T_c) electrons form Cooper pairs, and electrical resistivity becomes zero in the superconducting states.[1)] In addition, in the superconducting states, the electronic contribution to thermal conductivity (κ) is suppressed because the Cooper pairs, emerging in the superconducting states, do not transfer heat.[2)] The reduced κ in the superconducting states can be recovered to high κ by the application of magnetic field (H) greater than critical field (H_c) or upper critical field (H_{c2}) of the material, at which superconducting states are suppressed. Using the change in κ controlled by H, magneto-thermal switching (MTS) can be achieved by switching of the superconducting states. MTS is a key technology in the field of thermal management[3,4)] because the MTS can achieve heat flow control without any mechanical motions.[5,6)] Recently, we reported that large MTS ratio can be achieved in pure-element superconductors (Nb and Pb) with high purity.[7–9)] Although the working temperature of superconductor-based MTS should be low because the switching only happens below T_c, the MTS using low-T_c superconductors will be useful for thermal management of low-T devices,[10,11)] if the performance can be further improved. Furthermore, to make the MTS useful, it is necessary to develop materials with nonvolatile MTS in which high (or low) κ is retained even after removing external H. In Nb with intermediate states, nonvolatility was observed at low T,[2)] and the origin was explained as the affection of magnetic flux to phonon scattering. In the case of Nb intermediate states, the H experience resulted in lower κ. Recently, we achieved controllable large nonvolatile MTS in Sn-Pb solders.[12)] In the Sn-Pb solder, the nonvolatile MTS is driven by the change in electronic κ by the external H, and the switching ratio and the absolute value of κ can be controlled by Sn-Pb concentration and H.[12,13)] The Sn-Pb solders are known as phase-separated composites composed of Sn and Pb; both Sn and Pb are type-I superconductors with $T_c = 3.7$ and 7.2 K and H_c (0 K) $\sim$ 300 and 800 Oe, respectively.[14,15)] By field-cooling (FC) or reducing H from $H > H_c$, magnetic fluxes are trapped in the Sn regions, and bulk superconductivity of Sn is suppressed because of the trapped field greater than H_c of Sn.[12)] Similarly, magnetic flux trapping in MgB_2 ($T_c = 39$ K) causes nonvolatile MTS,[16)] but the switching ratio is smaller than that of Sn-Pb solders. Therefore, other examples of nonvolatile MTS in phase-separated composites using a superconducting transition have been desired to be studied because enrichment of examples of nonvolatile MTS will provide us with strategies for achieving a higher switching ratio of nonvolatile MTS. Here, we show the results on characterization, physical properties, and nonvolatile MTS characteristics of commercial In52-Sn48 solder, which is used in low-T soldering. The superconducting properties of In-Sn solders have been reported in Ref. 17 and the T_c of the solder is higher than that of pure In ($T_c = 3.4$ K) and Sn. According to the binary In-Sn phase diagram, phase separation into a β-phase (In-rich: $T_c = 6.5$ K) and γ-phase (Sn-rich: $T_c = 4.7$ K).[17)] Because of alloying states of those phases, the emergence of type-II superconductivity, in which quantized vortices are formed, in both regions are expected.[18–21)] If the vortex states can be retained after op [;'./ and demagnetization, and if nonvolatile MTS emerges, the material design space for nonvolatile MTS materials will be expanded because the most of the know superconducting materials are type-II superconductors. In addition, the use of type-II superconductors in nonvolatile MTS will improve working temperature and driving-field flexibility because of potential high Tc and critical fields in type-II materials. Therefore, we performed detailed characterization on the In52-Sn48 solder to obtain new insights on magnetic flux trapping and nonvolatile MTS in superconductor composites.

The investigated In52-Sn48 (mass ratio In:Sn = 52:48) commercial solder wires (Chip Quik Inc.) with a diameter of 0.79 mm. XRD was performed on a pressed sample in a plate form using a RIGAKU diffractometer Miniflex-600 with a Cu-Kα radiation by the θ–2θ method. SEM and EDX were performed using Carl Zeiss Cross-Beam 1540ESB for the micro-structure analysis with elemental mapping on the surface of the solder. Electrical resistivity (ρ) was measured using Physical Property Measurement System (PPMS, Quantum Design) with a four-probe method. Thermal conductivity (κ) was measured using PPMS with a thermal transport option (TTO) using a four-probe steady-state method with a heater, two thermometers, and base-temperature terminal. The lengths between two thermometers attached to the measured samples was 25.1 mm. Due to the limitation of the sample-room space of the TTO stage, the sample was screwed to store inside with four probes, a heater, two thermometers, and thermal base. The typical measurement duration for a single measurement was 30 s. Magnetization was measured using superconducting quantum interference device (SQUID) magnetometry on Magnetic Property Measurement System (MPMS3, Quantum Design) with a VSM mode. Specific heat was measured on PPMS by a relaxation mode. The sample was attached on a stage using APIEZON N grease.

Figure 1 shows the X-ray diffraction (XRD) pattern of the In52-Sn48 plate made by pressing the solder sample. A clear phase separation into the β-phase (In-rich, *I*4/*mmm*, No. 139) and γ-phase (Sn-rich, *P*6/*mmm*, No. 191) is seen, and no other impurity phases were observed. The crystal structure of the β-phase is same as pure In. Figure 2 shows the elemental mapping results based on scanning-electron microscope (SEM) and energy-dispersive X-ray spectroscopy (EDX). As shown in Figs. 2(c) and 2(d), clear and homogeneous phase separation into the two phases was observed. From the composition line analysis, the atomic composition of the β-phase can be estimated as $In_{0.68(2)}Sn_{0.32(2)}$, and that for the γ-phase is $In_{0.30(2)}Sn_{0.70(2)}$, which is consistent with the known phase diagram. The noticeable feature of the phase separation of the In52-Sn48 solder is presence of square-shaped γ-phase regions surrounded by the β-phase regions. The shape is different from the Sn-Pb solders studied in Ref. 12 However, the situation of lower-T_c regions surrounded by higher-T_c regions is similar to that of the Sn-Pb solders.

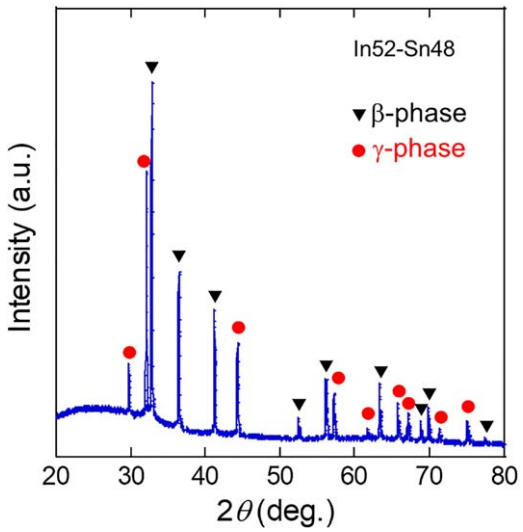

Fig. 1. X-ray diffraction pattern of In52-Sn48. The filled red circles and black triangles indicate the peaks for the γ-phase and β-phase, respectively.

Figure 3(a) shows the T dependence of magnetization ($4\pi M$) after zero-field cooling (ZFC) and FC with an applied magnetic field of $H = 10$ Oe. Large diamagnetic signals are observed at $T < 6.5$ K, which is consistent with the T_c of the β-phase. There is no double-step transition, while the In52-Sn48 sample contains two superconducting samples. This trend is quite similar to that observed in Sn-Pb solders, and the absence of double-step transition would be explained by the micro-scale phase separation and proximity effects.[12] Figure 3(b) shows the T dependence of $4\pi M$ measured at $H = 0$ Oe after FC at various H. By FC at 500 Oe, at $T = 1.8$ K and at $H = 0$ Oe, magnetic field of about 450 Oe is trapped. Furthermore, by FC at $H \geqslant 1000$ Oe, the trapped field of 620 Oe was observed, which indicates that the flux trapping saturates at $H = 1000$ Oe. Figures 3(c) and 3(d) show the H dependence of $4\pi M$ and inner magnetic field (B) at $T = 2.5$ K. As shown in Fig. 3(c), a typical hysteresis curve with an upper critical field of $H_{c2} \sim 1500$ Oe is observed at $T = 2.5$ K. Figure 4 shows the T dependence of electrical resistivity (ρ) measured at $H = 0$ Oe after FC at various fields. For all the FC conditions, almost same superconducting transitions were observed, which indicates that the resistive transition for the higher-T_c phase (β-phase) is not affected by the trapped vortices in the γ-phase regions.

To further investigate the superconducting properties of each phase, the specific heat was measured at different field conditions. Figure 5(a) shows the T dependence of specific heat (C) in the form of C/T measured at $H = 0$ Oe after ZFC and FC (3000 Oe). The C measurements were performed three times at each T. For the FC data, the first data point is masked because of anomalous sample heating related to flux reduction (anomalous temperature rise in the C measurements), which is the trend similar to Sn-Pb solders.[14] There is a slight difference in C/T between ZFC and FC data. To highlight the difference, normal-state C (C_n), which is shown in Fig. 5(b), is subtracted from the C/T data. Figure 5(c) shows the T dependence of $(C\text{-}C_n)/T$ calculated using C measured at $H = 0$ Oe after ZFC and FC (3000 Oe). At around $T = 6$ K, the superconducting signal is observed for both data, which indicates that the superconducting states of the ZFC and FC states are comparable down to 4.2 K. Therefore, the FC states of the β-phase would be close to Meissner states above $T = 4.2$ K. Below 4.2 K, there is a clear difference between the ZFC and FC data. In the ZFC data, there is a clear and sharp superconducting transition possibly of the γ-phase. In contrast, for the FC data, the superconducting transition of the γ-phase is clearly suppressed; the T_c is lower and the entropy change is smaller than that observed in the ZFC data. These results imply that the superconducting states of the γ-phase are affected by the presenting magnetic field, which is protected by the supercurrents of the β-phase, but the γ-phase is still bulk superconducting. If type-I superconducting states are emerging in the γ-phase, a first-order transition with a peak structure should be observed in specific heat data, but this is not the current case. In addition, as explained in the magnetization part, the $4\pi M$-H curve suggests type-II superconducting states. Therefore, the superconducting states of the γ-phase

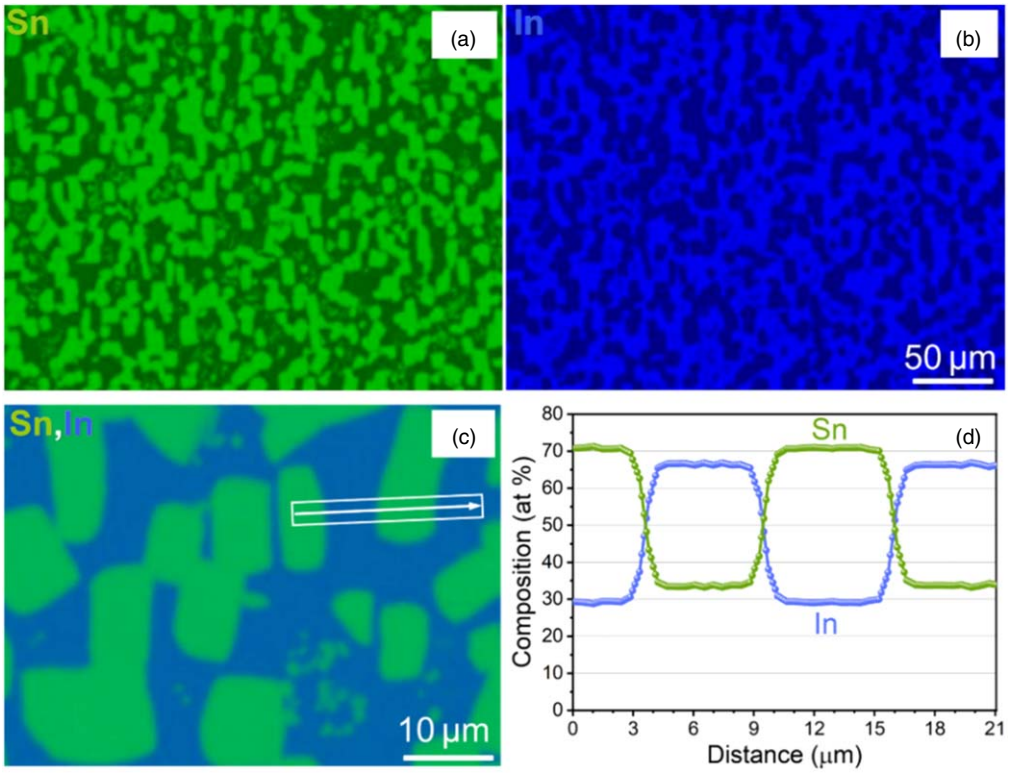

Fig. 2. Elemental mapping. (a), (b) SEM-EDX elemental mapping for Sn and In respectively. (c) Sn/In contrast mapping. (d) Composition line profile of constituent elements performed along the arrow in (c).

Table I. Comparison of nonvolatile MTS characteristics at $T = 2.5$ K. NMTSR, κ_i, κ_d, and κ_n denote nonvolatile magneto-thermal switching ratio, κ (initial value measured at $H = 0$ Oe after ZFC), κ (measured at $H = 0$ Oe after demagnetization), and κ (measured at $H > H_c$), respectively.

Material	Flux core	NMTSR	κ_i ($Wm^{-1}K^{-1}$)	κ_d ($Wm^{-1}K^{-1}$)	κ_n ($Wm^{-1}K^{-1}$)	References
Sn10-Pb90	No	300%	2	8	9.5	12
Sn45-Pb55	No	150%	10	25	34	12
Sn60-Pb40	Flux	56%	16	25	30	12
Sn90-Pb10	No	11%	27	30	43	12
In52-Sn48	No	45%	0.675	0.98	1.23	This work
In40-Sn60	No	11%	0.435	0.485	0.54	This work
In60-Sn40	No	59%	0.39	0.62	0.75	This work
MgB_2	—	18%	0.0070	0.0083	—	16

should be type-II state with vortices, and this situation is the clear difference from the case of Sn-Pb solders. The schematic image of the presence of vortices in the square-shaped γ-phase regions is displayed in Fig. 5(d).

As characterized in the above result part, the presence of type-II bulk superconducting states with vortices in the γ-phase surrounded by the β-phase with the Meissner state is clearly different from the situation of Sn-Pb solders where Sn is not bulk superconducting (when evaluating from the C measurement). Therefore, if we could observe nonvolatile MTS in the In52-Sn48 solder sample, the material design space will be largely expanded because of the availability of type-II superconductors as a component. Figure 6(a) shows the T dependence of κ measured at $H = 0$ (superconducting state) and 2000 Oe (normal-conducting state). There is a clear difference, and MTS can occur in the In52-Sn48 solder sample, which is caused by the switching of electronic κ between superconducting and normal-conducting states. In Fig. 6(b), the H dependence of κ measured at $T = 2.5$ K after initial ZFC is shown. After experiencing high fields $H > H_c$, external field is reduced to zero, but the κ at $H = 0$ Oe does not reach the initial κ. The κ-H result demonstrates the emergence of clear nonvolatile MTS in the In-Sn solder. The difference in κ between the before and after field experience (nonvolatile MTS ratio) is 45%. To investigate the composition dependence of MTS, we labo-made Inx-Sn(100-x) solders have been synthesized, and structural and physical properties were investigated (Supplementary Data). A similar phase separation, magnetic flux trapping, and nonvolatile MTS driven by electron contribution of κ were observed in $x = 40$ and 60.

Here, we investigated structural, compositional, and physical properties of the In-Sn solder. The solder traps a large amount of flux as observed in the Sn-Pb solders, but both phases are bulk superconducting even after FC, which indicates that, at least, the γ-phase is in type-II superconducting states with vortices. We observed nonvolatile MTS in the solder, and the switching ratio was 11%, 45% and 59% for In40-Sn60, In52-Sn48, and In60-Sn40, respectively. In Table I, nonvolatile MTS characteristics

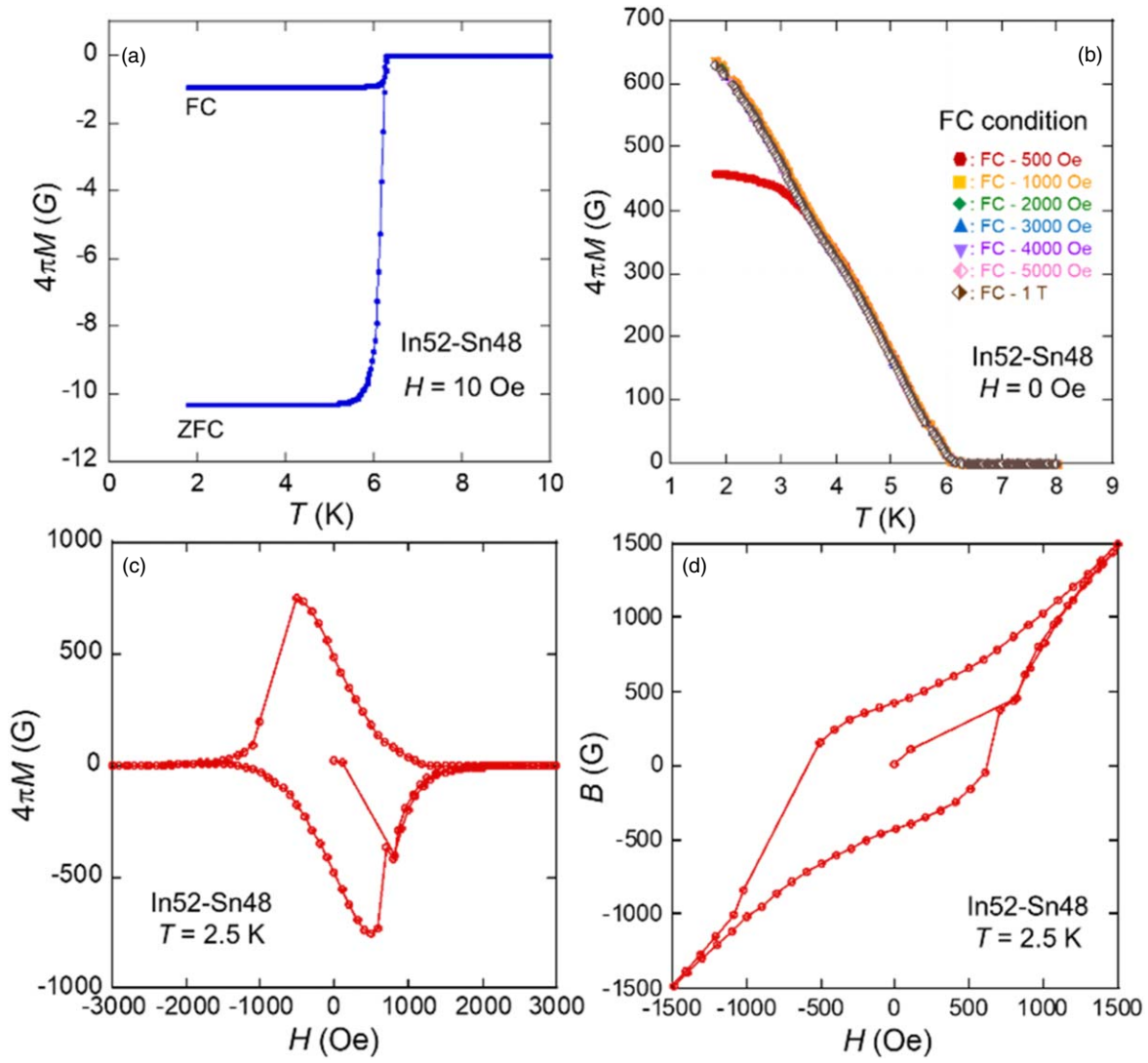

Fig. 3. Magnetic properties of In52-Sn48. (a) T dependence of $4\pi M$ after ZFC and FC with an applied field of $H = 10$ Oe. (b) T dependence of $4\pi M$ measured at $H = 0$ Oe after FC at various H. (c, d) H dependence of $4\pi M$ and inner magnetic field (B) at $T = 2.5$ K.

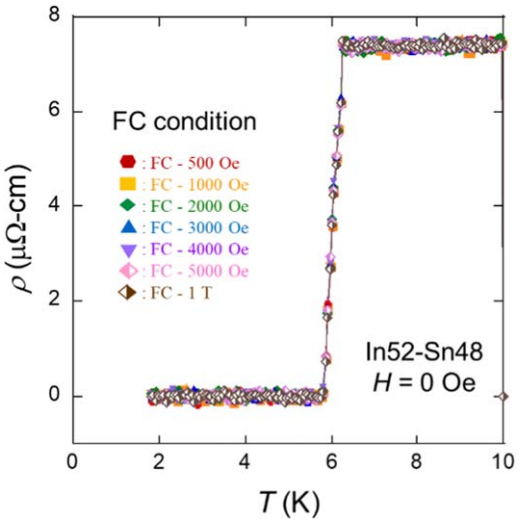

Fig. 4. Electrical resistivity after flux trapping. Temperature dependence of electrical resistivity of In52-Sn48 measured at $H = 0$ Oe after FC at various fields.

at $T = 2.5$ K for various materials are summarized. Nonvolatile MTS ratio (NMTSR) is defined by the following equation: NMTSR $= (\kappa_d - \kappa_i)/\kappa_i$ where κ_i and κ_d denote κ (initial value measured at $H = 0$ Oe after ZFC) and κ (measured at $H = 0$ Oe after demagnetization), respectively. The NMTSR of the In52-Sn48 solder at $T = 2.5$ K is smaller than typical values observed in the Pb-rich Sn-Pb solders (150% for Sn45-Pb55 and 300% for Sn10-Pb90) at $T = 2.5$ K, but NMTSR is comparable to that of Sn60-Pb40 flux-cored solder at $T = 2.5$ K. Furthermore, the NMTSR is greater than that for Sn-rich Sn90-Pb10 solder at $T = 2.5$ K. Therefore, type-II superconducting composites can be potential candidate for nonvolatile MTS materials as well as type-I-based composites. We notice that the κ of the In52-Sn48 commercial solder is quite low, which would be caused by the low κ of the constituent materials; alloys generally have lower κ than pure metals. As seen in Table I, the absolute values of κ of Sn-Pb solders[12] largely depends on the Sn-Pb compositions. Therefore, further optimization of In-Sn composition and material production processes would improve the MTS characteristics of In-Sn solders. Furthermore, this will allow us to design nonvolatile MTS materials with preferred value of κ by choosing the combination using pure metals, alloys, or complicated compounds in composite superconductors. At the end, but not least, the observation of nonvolatile MTS in a phase-separated superconducting composite containing a type-II superconductor expands the material-exploration space because of the

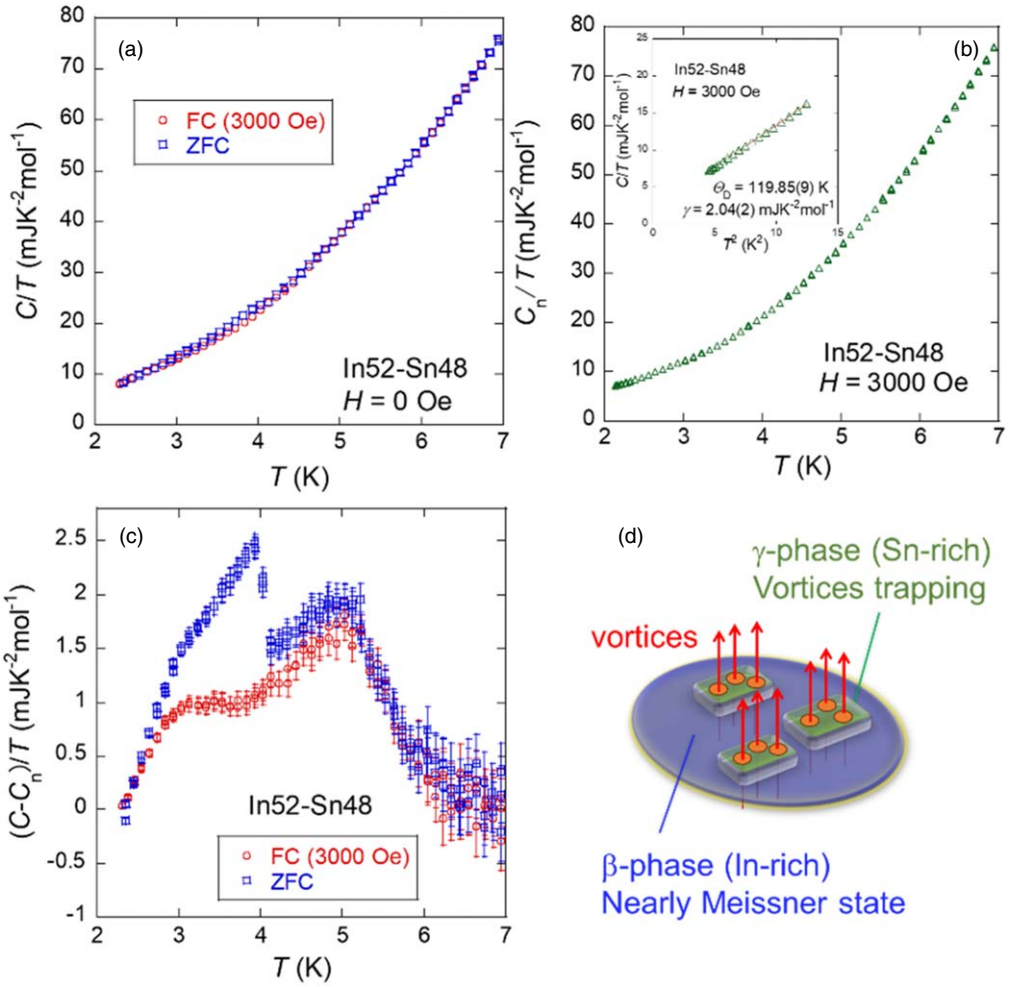

Fig. 5. Specific heat data for In52-Sn48. (a) T dependence of C/T measured at $H = 0$ Oe after ZFC and FC (3000 Oe). (b) T dependence of normal-state specific heat C_n/T. (c) T dependence of $(C\text{-}C_n)/T$ calculated using C measured at $H = 0$ Oe after ZFC and FC (3000 Oe). (d) Schematic image of vortex trapping at the γ-phase regions.

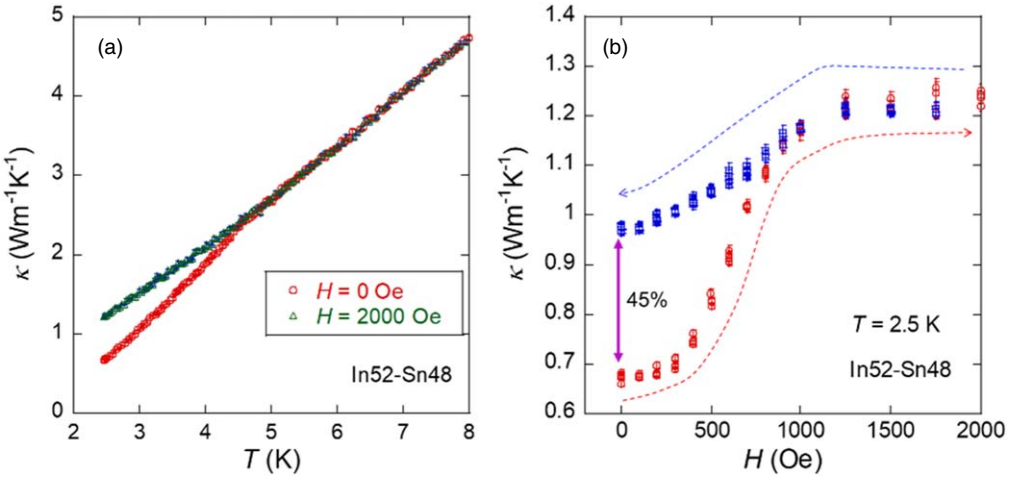

Fig. 6. Nonvolatile MTS of In52-Sn48. (a) T dependence of κ measured at $H = 0$ and 2000 Oe. (b) H dependence of κ measured at $T = 2.5$ K after ZFC.

availability of various superconductors. That is quite important for developing superconducting nonvolatile MTS using high-T_c superconductors.

In conclusion, we have investigated physical properties of the In52-Sn48 commercial solder which shows a clear phase separation into β-phase (In-rich: $T_c = 6.5$ K) and γ-phase (Sn-rich: $T_c = 4.7$ K). A large amount of magnetic flux trapping is observed in γ-phase after FC due to the presence of vortices in this region, which is confirmed by specific heat measurement that shows a clear suppression of the γ-phase superconducting transition temperature. Consequently, we observed a nonvolatile MTS in the solder with a 45% switching ratio. In addition, the switching ratio for labo-made In40Sn60 solder was 59%. The observation of nonvolatile MTS in a phase-separated type-II superconducting composite expands the exploration space for MTS materials.

Acknowledgments The authors thank F. Ando, K. Uchida, T. Ichikawa for the discussion on the results. This project was partly supported by TMU Research Project for Emergent Future Society and JST-ERATO (Grant No. JPMJER2201).

1) J. Bardeen, L. N. Cooper, and J. R. Schrieffer, Phys. Rev. **108**, 1175 (1957).
2) P. H. Kes, J. P. M. van der Veeken, and D. de Kierk, J. Low Temp. Phys. **18**, 355 (1975).
3) N. Li, J. Ren, L. Wang, G. Zhang, P. Hanggi, and B. Li, Rev. Mod. Phys. **84**, 1045 (2012).
4) G. Wehmeyer, T. Yabuki, C. Monachon, J. Wu, and C. Dames, Appl. Phys. Rev. **4**, 041304 (2017).
5) J. Kimling, J. Gooth, and K. Nielsch, Phys. Rev. B **91**, 144405 (2015).
6) H. Nakayama et al., Appl. Phys. Lett. **118**, 042409 (2021).
7) M. Yoshida, M. R. Kasem, A. Yamashita, K. Uchida, and Y. Mizuguchi, Appl. Phys. Express **16**, 033002 (2023).
8) M. Yoshida, H. Arima, A. Yamashita, K. Uchida, and Y. Mizuguchi, J. Appl. Phys. **134**, 065102 (2023).
9) M. Yoshida, H. Arima, Y. Watanabe, A. Yamashita, and Y. Mizuguchi, Physica C **623**, 1354536 (2024).
10) H. L. Huang, D. Wu, D. Fan, and X. Zhu, Sci. China Info. Sci. **63**, 180501 (2020).
11) M. Kjaergaard, M. E. Schwartz, J. Braumüller, P. Krantz, J-J. Wang, S. Gustavsson, and W. D. Oliver, Ann. Rev. Condens. Matter Phys. **11**, 369 (2020).
12) H. Arima, M. R. Kasem, H. S. Amin, F. Ando, K. Uchida, Y. Kinoshita, M. Tokunaga, and Y. Mizuguchi, Commun. Mater. **5**, 34 (2024).
13) Y. Mizuguchi, T. Murakami, M. R. Kasem, and H. Arima, EPL **147**, 36003 (2024).
14) J. D. Livingston, Phys. Rev. **129**, 1943 (1963).
15) S. Furuya, A. Tominaga, and Y. Narahara, J. Low Temp. Phys. **53**, 477 (1983).
16) H. Arima and Y. Mizuguchi, J. Phys. Soc. Jpn. **92**, 103702 (2023).
17) T. Mousavi, C. Aksoy, C. R. M. Grovenor, and S. C. Speller, Supercond. Sci. Technol. **29**, 015012 (2016).
18) A. A. Abrikosov, Rev. Mod. Phys. **76**, 975 (2004).
19) K. Harada, T. Matsuda, J. Bonevich, M. Igarashi, S. Kondo, G. Pozzi, U. Kawabe, and A. Tonomura, Nature **360**, 51 (1992).
20) H. F. Hess, R. B. Robinson, and J. V. Waszczak, Physica B **169**, 422 (1991).
21) F. S. Wells, A. V. Pan, X. R. Wang, S. A. Fedoseev, and H. Hilgenkamp, Sci. Rep. **5**, 8677 (2015).